

**END-REGION CRACKING IN PRETENSIONED CONCRETE GIRDERS
EMPLOYING 0.7-IN. STRANDS: TIME-DEPENDENT AND SERVICE-LOAD
EFFECTS**

Hyun su Kim, The University of Texas at Austin, Austin, TX

Rodolfo Bonetti, The University of Texas at Austin, Austin, TX

Alistair Longshaw, The University of Texas at Austin, Austin, TX

Hossein Yousefpour, Ph.D., Babol Noshirvani University of Technology, Babol, Iran

Trevor Hrynyk, Ph.D., The University of Texas at Austin, Austin, TX

Oguzhan Bayrak, Ph.D., P.E., The University of Texas at Austin, Austin, TX

ABSTRACT

The use of 0.7-in. diameter strands instead of 0.5- or 0.6-in. diameter strands in pretensioned girders results in greater end-region stresses that can lead to cracking. End-region cracks, which might negatively affect the durability and strength of girders, develop at prestress transfer and change in length, width, and number over time and under applied loads. This paper investigates the effects of applied loads and time-dependent volumetric changes of concrete on cracking conditions within the end-regions of Texas bulb-Tee girders (Tx-girders) that employ 0.7-in. diameter strands on a 2- by 2-in. grid. A series of full-scale specimens was fabricated at Ferguson Structural Engineering Laboratory and was subjected to shear-critical loading at an age of 28 days or greater. The specimens were well-instrumented to estimate the end-region stresses at the time of prestress transfer. Crack widths and patterns, as well as prestress losses, were also monitored throughout the life of the specimens, including the duration of the shear tests. The number and width of cracks increased noticeably within the first three weeks after prestress transfer. However, the widths of most web cracks were reduced nearly by half under relatively small applied loads. The results provide valuable insight into acceptance limits for end-region cracks to ensure serviceable and durable pretensioned girders.

Keywords: 0.7-in. Strands, Prestressed Concrete, End-Region Crack, Long-Term Effect, Service-Load

INTRODUCTION

In recent years, the use 0.7-in. diameter prestressing strands in pretensioned concrete elements instead of the commonly employed 0.5- or 0.6-in. diameter strands has garnered considerable interest. This transition could potentially reduce the fabrication costs by reducing the number of required strands and improve the flexural efficiency of pretensioned girders by allowing a greater steel area to be concentrated near the bottom of the cross section. However, the implementation of these larger-diameter strands can potentially have negative effects on the serviceability and strength of girders.

End-regions of pretensioned girders are subjected to transverse stresses that are categorized as bursting and spalling stresses. Bursting stresses develop primarily in the bottom flange of the girders when the prestressed strands tend to return to their original diameter at the time of release. Excessive bursting stresses may result in longitudinal cracking at the elevation of strands. Spalling stresses develop as a result of the compatibility of strains near the end face. These stresses depend on the eccentricity of strands from the centroid of the cross section and can cause horizontal or inclined cracking in the web at an elevation away from the strands.

Excessive cracking due to bursting and spalling stresses might have negative effects on the strength, serviceability, and durability of pretensioned girders. Cracks at the locations of strands could potentially affect bond stresses between the strands and concrete and, hence, affect the load-carrying capacity of the member¹. Moreover, water or de-icing agents might permeate through the end-region cracks and cause corrosion in strands or mild-steel reinforcement. Therefore, appropriate reinforcement detailing is needed within the end-regions of pretensioned elements to control the widths of bursting and spalling cracks. The use of larger-diameter 0.7-in. strands is expected to increase the end-region stresses, which may lead to increased end-region damage in pretensioned concrete elements. Therefore, employing 0.7-in. diameter strands may require modifying the end-region reinforcement and therefore revisiting the acceptable crack widths within the end-regions of the girders,

Acceptable widths for flexural cracks have been the subject of a number of previous studies and design guidelines, as reported in Tables 1 and 2. However, the criteria presented in these tables might not be directly applicable to end-region cracks. Flexural cracks tend to grow under applied loads, whereas previous experimental evidence¹ suggests that end-region cracks may actually reduce in width due to applied loads. Moreover, the criteria presented in Tables 1 and 2 restrict the crack widths under service-load conditions. Therefore, it is of interest to investigate changes that happen in the cracking conditions from the time of fabrication until the time the girder is put in service condition so that a reliable set of criteria can be developed for accepting or rejecting a girder based on the observed crack widths immediately after prestress transfer.

Table 1 Summary of acceptable crack widths from previous studies and design guidelines

Researcher or Organization	Exposure condition	Tolerable crack width, in. (mm)
Nawy ²	Dry air or protective membrane	0.016 (0.41)
	Humidity, moist air, soil	0.012 (0.30)
	Deicing chemicals	0.007 (0.18)
	Seawater and seawater spray, wetting and drying	0.006 (0.15)
	Water-retaining structures	0.004 (0.10)
Halvorsen ³	For aesthetics & structural safety	0.006 (0.15)
PCI ⁴	Exposed to humidity	0.012 (0.30)
	Subjected to deicing chemicals	0.007 (0.18)
	Exposed to sea water and seawater spray, wetting and drying cycles	0.006 (0.15)

Table 2 Acceptable crack widths according to CEB EN2⁵

Exposure condition	Maximum crack width at extreme tensile fiber of the concrete section, in. (mm)	90 th percentile of the crack width, in. (mm)
Severe: <ul style="list-style-type: none"> • Corrosive gasses or soils • Corrosive industrial or maritime environment 	0.012 (0.3)	0.004 (0.1)
Moderate: <ul style="list-style-type: none"> • Running water • Inclement weather without aggressive gasses 	0.016 (0.4)	0.008 (0.2)
Mild: <ul style="list-style-type: none"> • Conditions where high humidity is reached for a short period in any one year 	0.020 (0.5)	0.012 (0.3)

The objective of this paper is to investigate the effects of time-dependent volumetric changes of concrete, as well as the effects of applied loads, on end-region cracks in Texas bulb-Tee girders (Tx-girders) that employ 0.7-in. diameter strands on a 2- by 2-in. grid. The research presented in this paper involves fabrication and structural testing of a series of full-scale specimens, as well as nonlinear finite element analyses (FEA). The experimental program involving the fabrication and testing of the full-scale specimens is introduced first, followed by an overview of the work done to monitor the cracking conditions within the end-regions of the specimens. Next, finite-element simulations conducted to evaluate the changes in cracking under load are introduced. Finally, the experimental and computational results are presented and discussed to obtain insights into changes in end-region cracks over time and under loads.

EXPERIMENTAL PROGRAM

As part of a comprehensive research program at the University of Texas at Austin, seven full-scale specimens were fabricated and tested at Ferguson Structural Engineering Laboratory (FSEL) to investigate the end-region behavior and shear strength of pretensioned concrete girders constructed with 0.7-in. diameter strands on the standard 2- by 2-in. grid^{6,7,8}. Three out of these seven specimens were selected for evaluating how end-region cracks were affected by time-dependent volumetric changes and service loads. The design, fabrication, and testing of these specimens, which are herein referred to as Tx70-II, Tx46-IV, and Tx46-V, are introduced in this section.

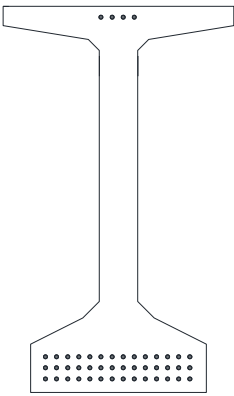
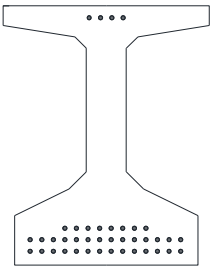
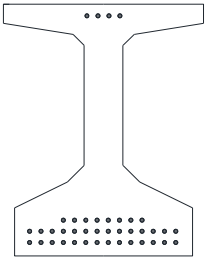
SPECIMEN DESIGN AND FABRICATION

A summary of the details for the three specimens presented this paper is shown in Table 3. In all cases, the specimens were 30-ft long and were fabricated using the prestressing facility at FSEL. Stressing and release of prestressing strands at this facility are performed through gradual extension and retraction of hydraulic rams. Throughout this paper, the end of the specimen located near the hydraulic rams is referred to as the live end whereas the specimen end coinciding with the fixed stressing plate is referred to as the dead end.

It is generally reported that that a gradual transfer of prestress may result in shorter transfer lengths compared with a sudden release method^{9,10}. While hydraulic release of prestressing is becoming more common in prestressing facilities, many precast concrete manufacturers still use flame cutting to release the prestressing force. However, even in the case of flame-cutting the strands, it is required by most construction specifications that the wires comprising 7-wire strands be cut individually and slowly, resulting in a gradual prestress transfer. Therefore, the use of hydraulic release provides a reasonable representation of conditions of girders in the field. Moreover, previous experimental evidence¹¹ has indicated that prestress release method has a less noticeable effect on pretensioned girders with high concrete release strengths.

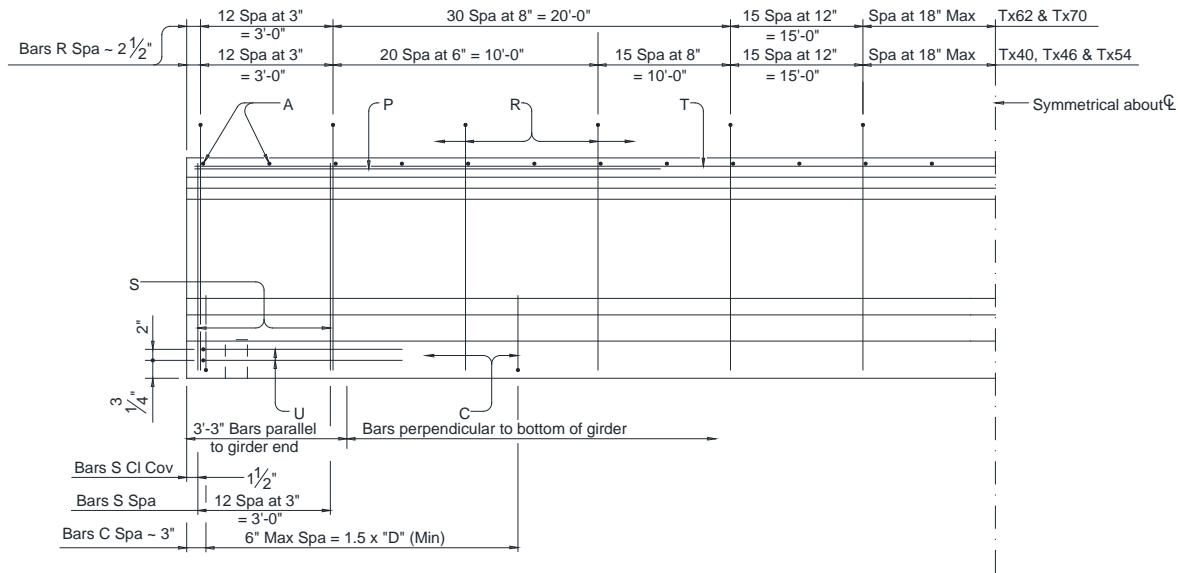
All specimens employed straight 0.7-in. diameter prestressing strands that were placed on a standard 2- by 2-in. grid. To maximize the flexural capacity of the specimens and create critical conditions for spalling stresses, the strands in the bottom flange were placed at the greatest possible eccentricity in each specimen. Each specimen also contained four 0.7-in. diameter strands within the top flange to control the stresses at the time of prestress transfer. Parametric studies by Salazar et al.¹² showed that increasing the release strength of concrete, to a minimum of 7.5 ksi, can provide noticeable benefits in terms of additional flexural capacity when using 0.7-in. diameter strands. Therefore, the specimens were designed assuming a concrete release strength on the order of 8 ksi, which is greater than what is typically used in the industry. The specimens were designed according to the 2016 interim revisions to AASHTO LRFD Bridge Design Specifications¹³.

Table 3 Summary of specimen design properties

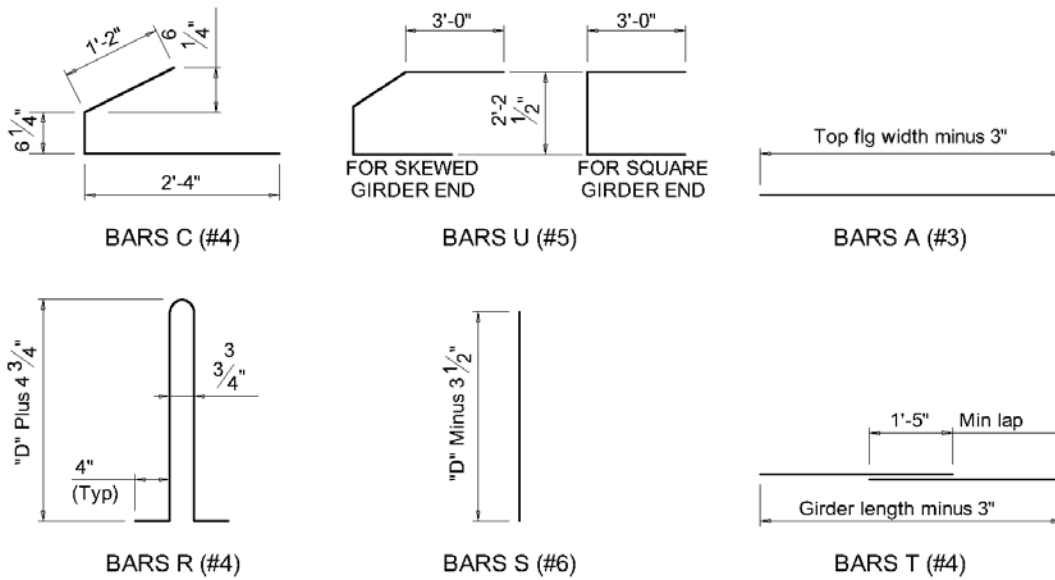
Design properties	Tx70-II	Tx46-IV	Tx46-V
Cross section			
Design f'_{ci} [ksi]	7.8	8.0	8.0
Effective depth from top* [in.]	65.5	41.8	41.8
Number of top strands	4	4	4
Number of bottom strands	42	36	36
Jacking stress for bottom strands [ksi]	202.5	202.5	202.5
Jacking stress for top strands [ksi]	202.5	165.0	165.0
End-region modification	None	Use Larger Transverse Reinforcement	Add Horizontal Bars

* Cast-in-place slab not included

The first specimen, Tx70-II, was designed and detailed according to the standard drawings currently used by the Texas Department of Transportation (TxDOT) for Tx-girders with smaller-diameter strands¹⁴, which is shown in Fig. 1. Tx46-IV and Tx46-V had similar designs in terms of prestressing layout and concrete release strength. However, the end-region detailing was modified in these two specimens in an effort to reduce the width and number of end-region cracks and control the strand slip under applied loads. In Tx46-IV, the diameter of S-bars (shown in Fig. 1) at the dead end was increased from No. 6 to No. 8. Tx46-V contained No. 6 S-bars, but as shown in Fig. 2, a series of horizontal No. 4 bars were added within the web of this specimen at the dead end to help restrain the growth of inclined spalling cracks. Moreover, Tx46-V contained “cap bars” at both ends to more effectively confine the bottom flanges and assess the impacts of strand confinement on the shear capacity and the ductility of the girders.



(a) Elevation view



(b) Reinforcing bars details

Fig. 1 Standard TxDOT detailing for end-region reinforcement in Tx-girders¹⁴

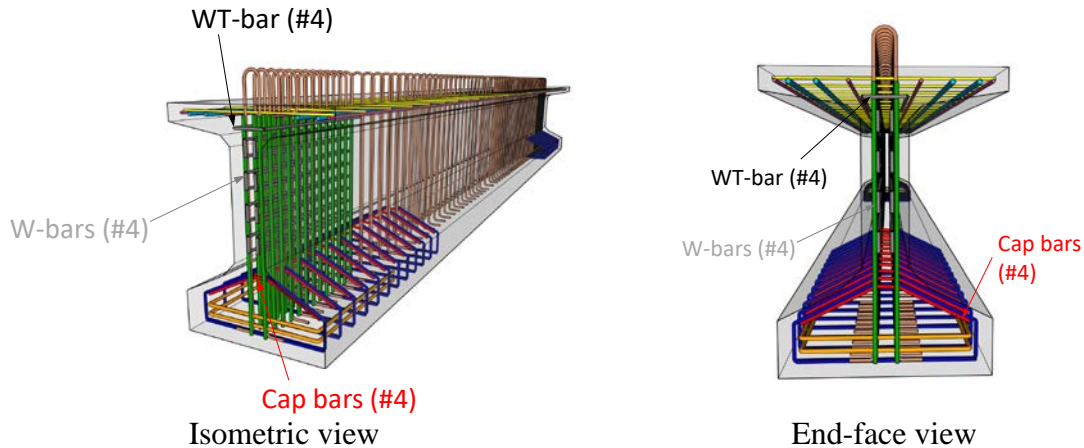


Fig. 2 Modification to reinforcement in the end-region of Tx46-V

Fig. 3 shows an overview of the fabrication process for the specimens. Reusable strand chucks were used for anchoring the 0.7-in. diameter strands at each end on a 2- by 2-in. grid. Initially, each strand was individually stressed to remove the slack and ensure uniform stressing of the strands. After the slack was removed, all strands were gang-stressed, i.e. stressed together, in 10 increments using hydraulic rams, during which the hydraulic pressure in the rams was carefully monitored. The elongation of the strands was also monitored using a series of linear potentiometers at each end of the prestressing facility and verified to be within 5 percent of the calculated value at the completion of each stressing increment.

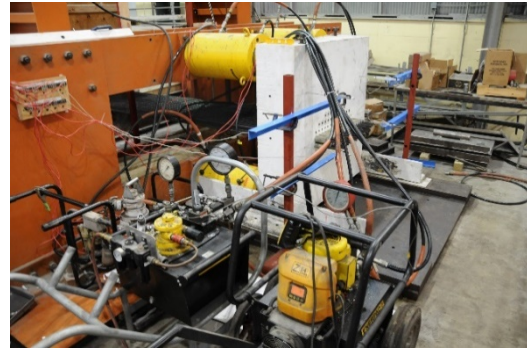
Once the strands were stressed to the desired level, installation of the transverse reinforcement and instrumentation was carried out. Strain gauges were installed on transverse reinforcement to measure strains in the stirrups and on strands to estimate transfer length. Vibrating wire strain gauges (VWGs) were also placed at the midspan locations of the girders to measure the strains due to time-dependent effects and prestress losses.

To represent the conditions of pretensioned concrete girders in the field, the concrete mixture used within the specimens contained Type III cement, which was batched and mixed by Coreslab Structures in Cedar Park, Texas and transported to FSEL. Forty-eight, 4 by 8 in., match-curing concrete cylinders were cast using the concrete comprising each specimen. These cylinders were cured at the same temperatures as those measured from thermocouples embedded in the specimens. In the hours following the concrete placement, match-cured specimens were periodically tested to identify the appropriate timing for prestress transfer. Prestress transfer commenced as soon as the compressive strength of match-cured cylinders corresponding to all thermocouple locations exceeded the design release strength.

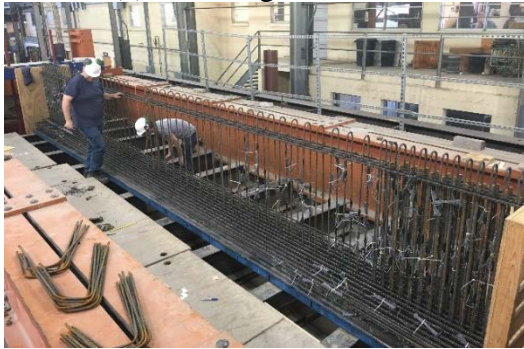
The strands were released through gradual retraction of the hydraulic rams over 20 steps, which typically took approximately one hour. While the strands were being released, the compressive strength and modulus of elasticity were measured to obtain the mechanical properties at prestress transfer, which are presented in Table 4.



(a) Installing the strands



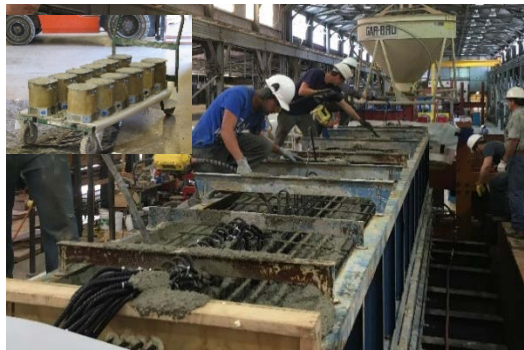
(b) Gang-stressing the strands



(c) Installing the reinforcement and instrumentation



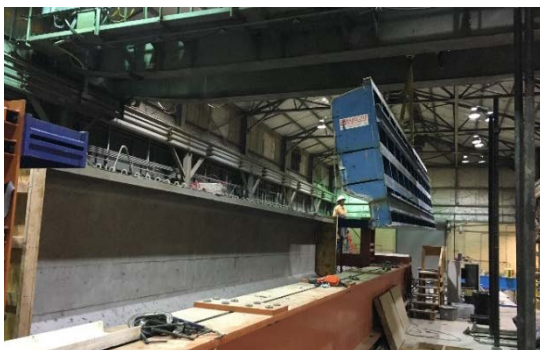
(d) Closing side forms



(e) Casting the specimen



(f) Periodic testing of match-cured cylinders



(g) Removing the side forms



(h) Prestress transfer and inspection

Fig. 3 Specimen fabrication process

Table 4 Summary of concrete mechanical properties at the time of release

Mechanical Property	Tx70-II	Tx46-IV	Tx46-V
Concrete Release Strength, f'_{ci} [ksi]	8.3	8.4	8.5
Modulus of Elasticity of Concrete, E_c [ksi]	4,900	5,650	5,800

SHEAR TEST

Within two weeks after prestress transfer, a reinforced concrete slab was constructed on each specimen to simulate a bridge deck, distribute the applied loads effectively, and increase the flexural capacity of the specimens. The slab had a thickness of 8 in. and a width that was 2 in. less than that of the top flange of the precast section.

The specimens were tested in a simply supported, shear-critical loading configuration, which is shown in Fig. 4. To examine potential differences between the behavior of the live and dead ends and to ensure a consistent shear span-to-depth ratio that does not depend on the failed span, the specimens were subjected to a symmetric loading configuration, in which both ends of the specimen were subjected to equal shear forces. The shear span-to-depth ratio was 2.3 for Tx70-II and 3.0 for the Tx46 specimens. The concrete comprising the specimens had a minimum age of 28 days at the time of shear testing. Measured mechanical properties of the concrete on the test day and those of the reinforcing bars are summarized in Table 5.

Table 5 Summary of material properties at the time of shear test

Variables	Tx70-II	Tx46-IV	Tx46-V
Concrete strength, f'_c [ksi]	12.7	13.9	14.5
Modulus of elasticity of concrete, E_c [ksi]	6,000	6,050	7,500
Yield strength of shear reinforcement, f_y [ksi]	72.2	63.1	64.1

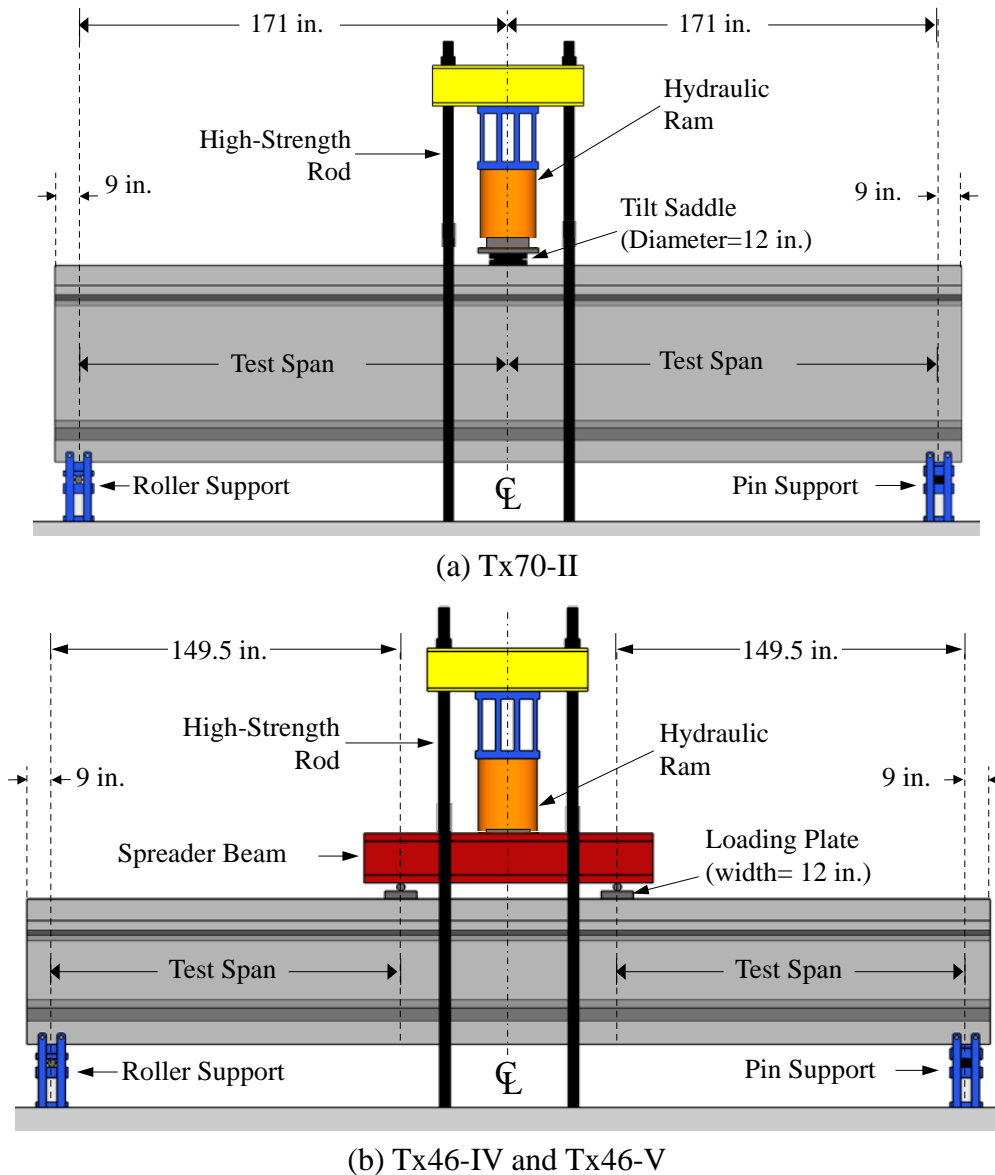


Fig. 4 Loading configuration for shear test

Load was applied to the specimens using a 2,000-kip hydraulic ram that was pressurized by a pneumatically controlled hydraulic pump. A series of load cells installed at the supports was used to measure the reaction forces during the test and linear potentiometers installed at each loading point and each support were used to monitor the vertical deflections of the specimen. The applied load was increased in 100-kip increments. After each increment, the conditions of cracks within the end-regions and those in the shear span were inspected and documented. After considerable diagonal cracking occurred due to applied load, the specimens were continuously loaded to failure while recording the data from the instrumentation.

CRACK MONITORING

The specimens were thoroughly inspected for cracks throughout their lengths immediately after prestress transfer. The widths of these cracks were measured at several points using a magnifying loupe (Fig. 5a) with reticles that provided a resolution of 0.004 in. For cracks that were wider than 0.006 in., a crack-comparator gauge with a resolution of 0.002 in. was employed (Fig. 5b). For each specimen, measurements of widths and patterns of the cracks were repeated at ages of 1, 7, 14, 21, and 28 days, as well as immediately before the shear test. During each set of measurements, changes in the number, lengths, and the widths of cracks were carefully documented. As a result, a clear picture of the evolution of end-region cracks over the first 28 days of the life of the specimen could be obtained.

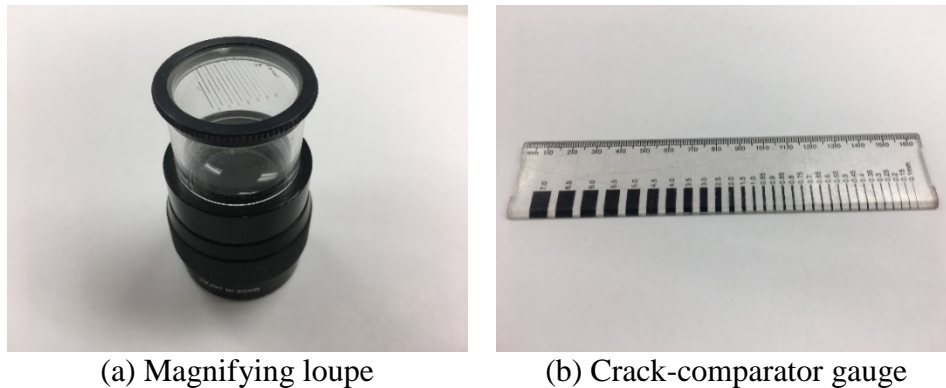


Fig. 5 Crack measurement tools

The widths of end-region cracks were measured during the shear tests of Specimens Tx46-IV and Tx46-V. For Tx46-IV, the crack widths were measured at applied loads of 200, 300, 400, and 495 kips, which corresponded to the appearance of first diagonal shear crack. Tx46-V was monitored more rigorously, with the crack widths measured after the application of each 100-kip increment, until reaching an applied load of 900 kips. The crack widths were also recorded immediately after the first diagonal cracking in this specimen (545 kips).

For Tx46-V, in addition to visual measurements of crack widths, a series of strain measurements was made during the shear test, using a Demountable Mechanical strain gauge (DEMEC gauge). DEMEC markers were installed on both faces of each end-region, at the locations that could represent the greatest crack width that was identified through visual measurements. The markers were placed equidistantly on either side of the cracks to measure the surface strain perpendicular to the crack direction.

FINITE ELEMENT ANALYSIS (FEA)

To improve the understanding of end-region cracks due to prestress transfer and changes in these cracks due to long-term and service-load effects, a series of nonlinear finite element analyses was performed using ATENA-3D¹⁵, a commercial FEA software program that is specialized for simulating reinforced concrete structures. Models of pretensioned concrete girders with 0.7-in. diameter strands were developed and validated through comparison with

experimental results from previous studies by O'Callaghan¹⁶, Tadros and Morcous¹⁷, and the current research program.

The primary input variable for the mechanical properties of concrete was the compressive strength at the times of release and shear-critical loading test. Other concrete mechanical parameters were automatically calculated by ATENA, on the basis of the concrete compressive strength. The behavior of the reinforcing bars and prestressing strands was assumed to be bilinear with strain hardening using the mechanical properties that were measured according to ASTM A370¹⁸. The Bigaj bond model¹⁹ was applied to simulate the bond between the concrete and prestressing strands, while all other reinforcing bars were assumed to have perfect bond with the surrounding concrete.

Fig. 6 shows the typical mesh that was used for the specimens. Following a mesh sensitivity analysis, each specimen was simulated with a typical element size of 1.97 in. The entire length, but half of the width of each specimen was modeled. Crack widths and patterns were computed after the prestress transfer and during each load step at the time of shear test. Shear-critical loading tests were simulated using a displacement-controlled loading scenario.

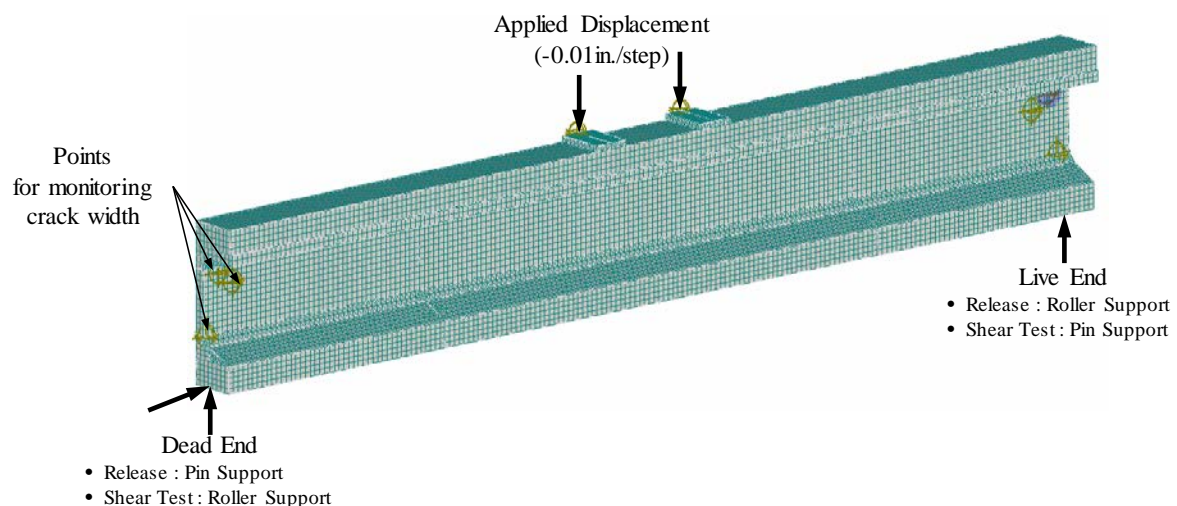


Fig. 6 Typical FE mesh for Tx-girders employing 0.7-in. strands

RESULTS AND DISCUSSION

END-REGION CRACKS IMMEDIATELY AFTER PRESTRESS TRANSFER

All specimens were carefully inspected for cracks immediately after prestress transfer. The measured cracking patterns of the specimens are shown in Fig. 7, Fig. 8, and Fig. 9. These figures illustrate the end faces and both sides of the live and dead ends of the specimens. The specimens were aligned in the north-south direction, with the dead end located at south. The small circles in the figures represent the measured widths of the cracks at each location. In the regions where no circles are shown, the crack width was less than or equal to 0.004 in.

The specimens showed clear patterns of spalling cracks within their end-regions. All specimens showed near-continuous cracking at the interface between the web and the bottom flange within the end-region and through the width of the web at the end faces. In Tx70-II and Tx46-V, cracks parallel to the outermost strands were also observed, which is indicative of bond-related damage.

In general, the difference in patterns or widths of cracks between the live and dead ends was not significant in any of the specimens. The maximum crack width recorded immediately after prestress transfer among the three specimens was approximately 0.006 in. This crack width was observed in one of the spalling cracks within the web of Tx70-II. However, crack widths between 0.005 and 0.006 in. were measured at several locations in this specimen. A maximum crack width of approximately 0.005 in. was observed in Tx46-IV and Tx46-V. This maximum width was observed in the spalling cracks in the web for Tx46-IV but at the interface between the bottom flange and the web for Tx46-V.

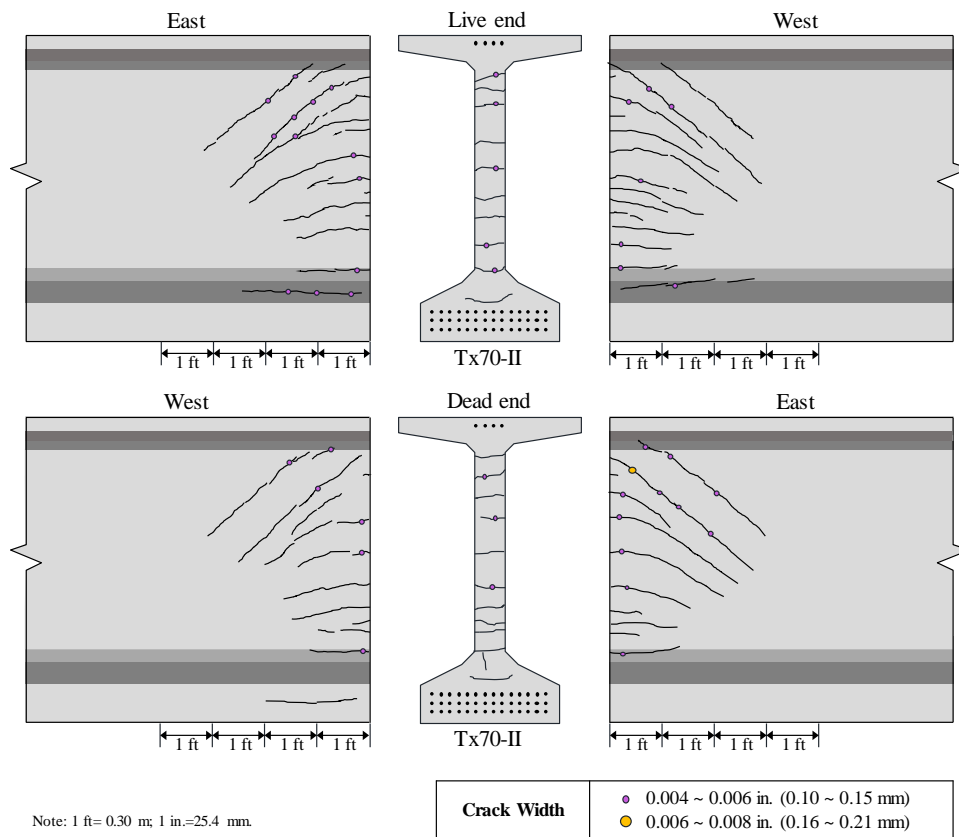


Fig. 7 End-region cracks within Tx70-II immediately after prestress transfer

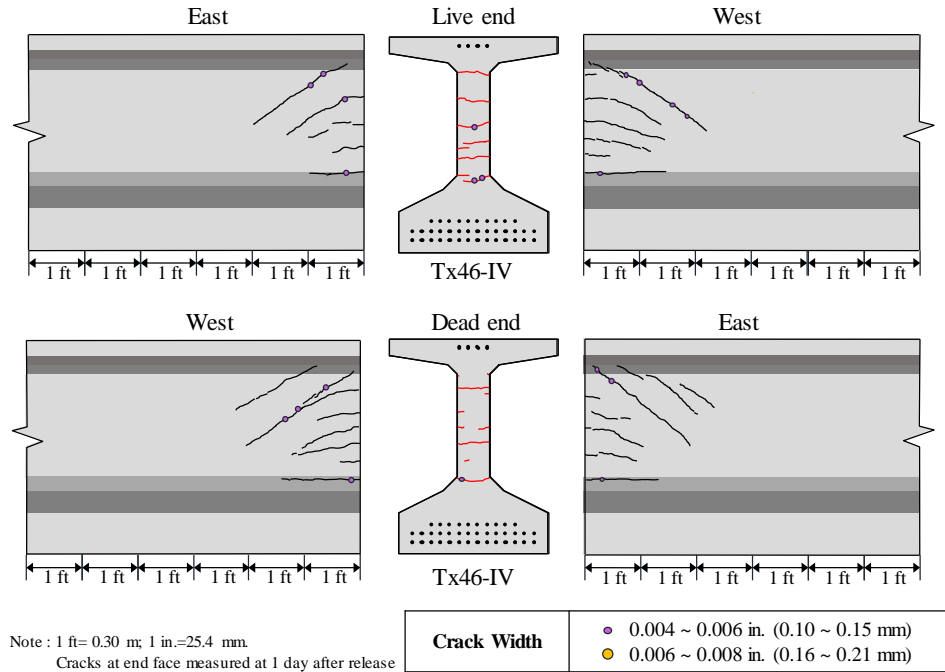


Fig. 8 End-region cracks within Tx46-IV immediately after prestress transfer

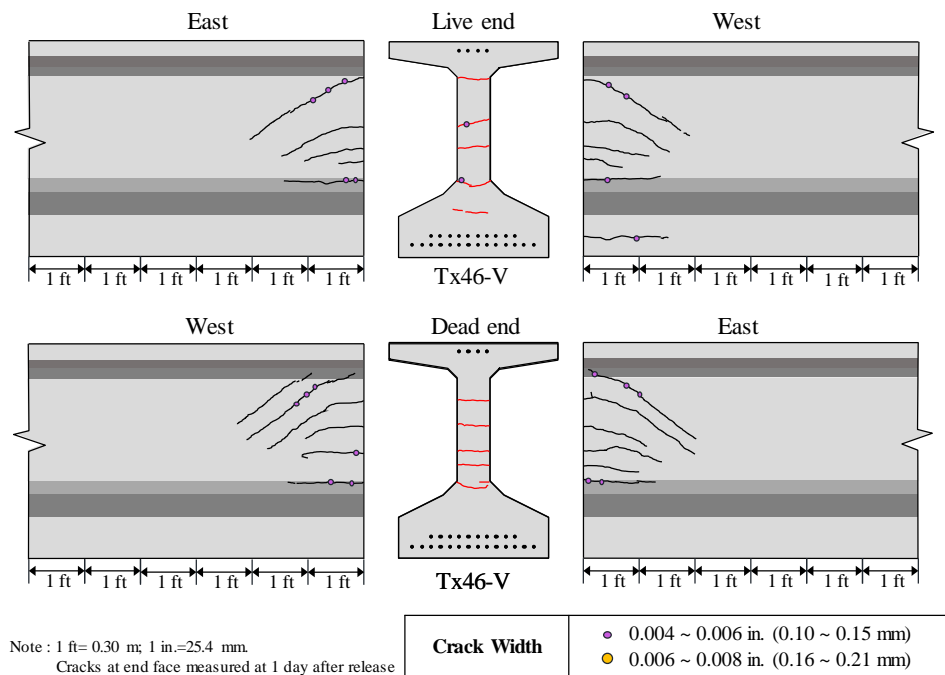


Fig. 9 End-region cracks within Tx46-V immediately after prestress transfer

TIME-DEPENDENT CHANGES IN CRACK WIDTHS

All specimens demonstrated noticeable changes in their cracking conditions over time, as shown in Fig. 10, Fig. 11, and Fig. 12. These changes included growth in the length and width of cracks that were initially detected after prestress transfer, as well as the development of new

cracks in all specimens. Typically, the greatest crack widths and the greatest change in the crack width were observed in the longest inclined spalling crack, which started at the intersection of the top flange and the web. The greatest crack widths were observed within the first 18 in. from the end faces of the beam.

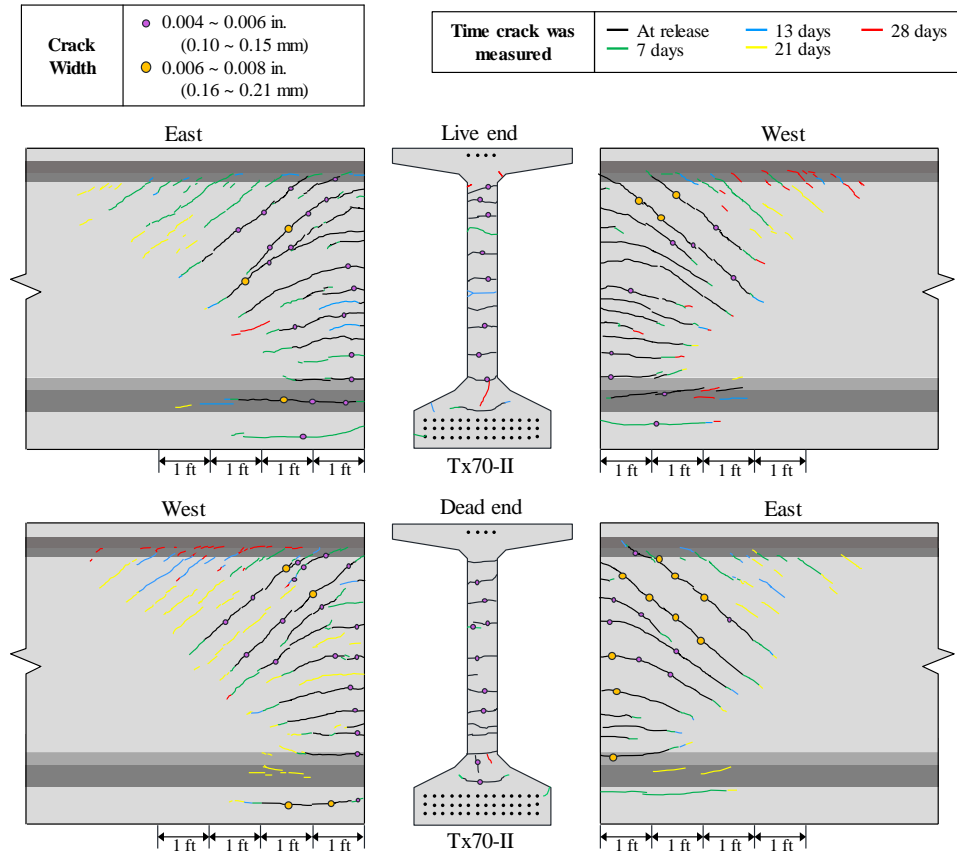


Fig. 10 Evolution of end-region cracks within Tx70-II

A maximum crack width of 0.006 in. was observed in one location at the dead end of Tx70-II immediately after prestress transfer. However, 28 days after prestress transfer, a crack width of 0.006 in. was measured at several locations along the spalling cracks at both ends. The crack width at some locations in the dead end of this specimen reached 0.007 in.

After release, a maximum crack width of 0.005 in. was observed at both dead and live ends of Tx46-IV. However, the last documented measurements from this specimen, which were taken 62 days after release, revealed a crack width of 0.008 in. at the live end, as shown in Fig. 11. The crack patterns and widths showed no significant benefit from the use of No. 8 S-bars instead of No. 6 bars in this specimen.

For Tx46-V, a maximum crack width of 0.005 in. was observed at both dead and live ends immediately after prestress transfer. As shown in Fig. 12, the last documented measurements from this specimen, which were made 28 days after release, revealed a crack width of 0.006 in. at several locations at both ends. The horizontal crack control reinforcement in the end-region

did not provide any noticeable benefits pertaining to crack patterns and widths.

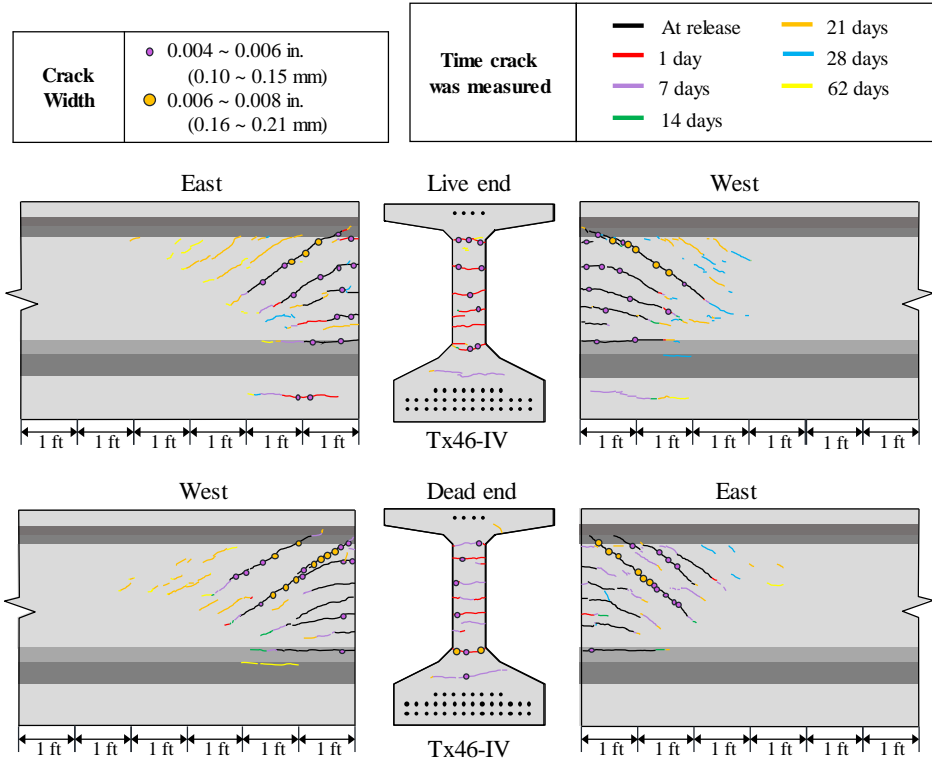


Fig. 11 Evolution of end-region cracks within Tx46-IV

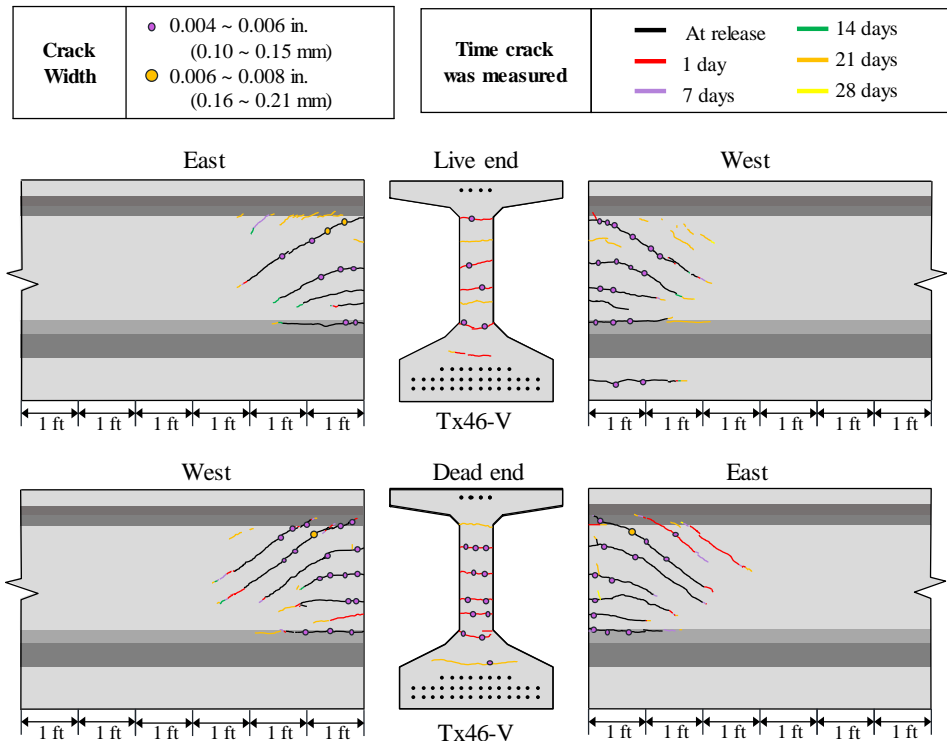


Fig. 12 Evolution of end-region cracks within Tx46-V

There is no globally accepted limit for the permissible crack width within the end-regions of pretensioned concrete elements. ACI 224R²⁰, a report developed by the ACI committee on concrete cracking, provides general guidelines on acceptable crack widths in reinforced concrete flexural elements under service loads. According to these guidelines, the limit on crack width is 0.007 in. for elements exposed to deicing chemicals and 0.012 in. for elements exposed to humidity, moist air, and soil. A comprehensive study on the acceptance criteria for the width of end-region cracks by Tadros, Badie, and Tuan¹ also recommends that no action be taken for any cracks that are smaller than 0.012 in. in width.

The observed crack widths in this study did not exceed the recommended 0.012-in. limit requiring repair. Moreover, no cracks within the end-regions of the girders exceeded the same 0.012-in. limit recognized by ACI 224R as tolerable for humidity and soil exposure. However, as noted by ACI 224R, a few cracks with widths greater than the listed limits are considered acceptable. Therefore, according to ACI 224R, all girders comprising this test program met the conditions for use in exposure to deicing chemicals.

For the subsequent results and discussions presented in this paper, the cracks within the end-regions of the specimens are identified using the notation shown in Fig. 13 through Fig. 15.

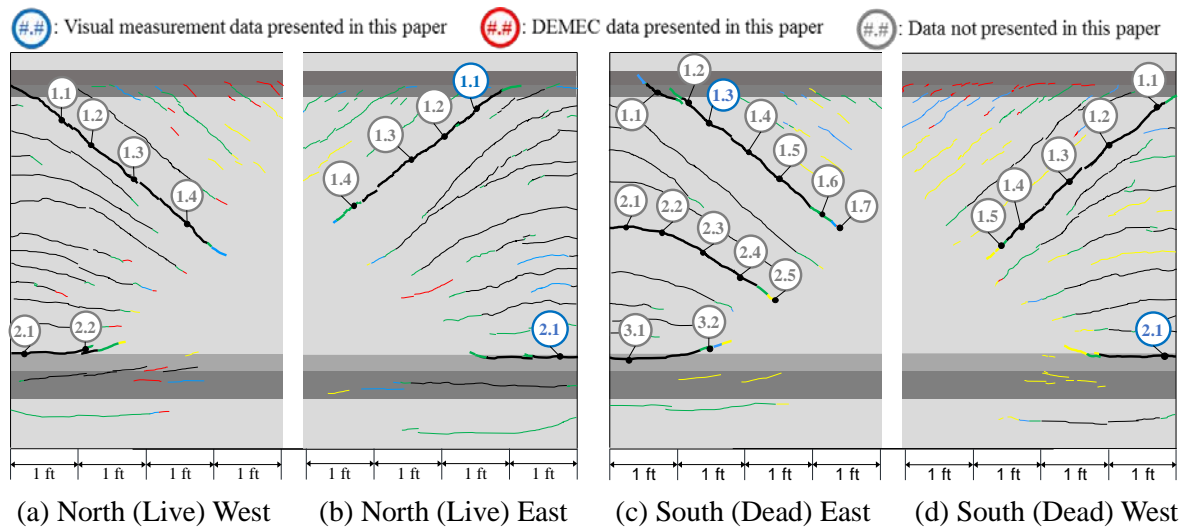
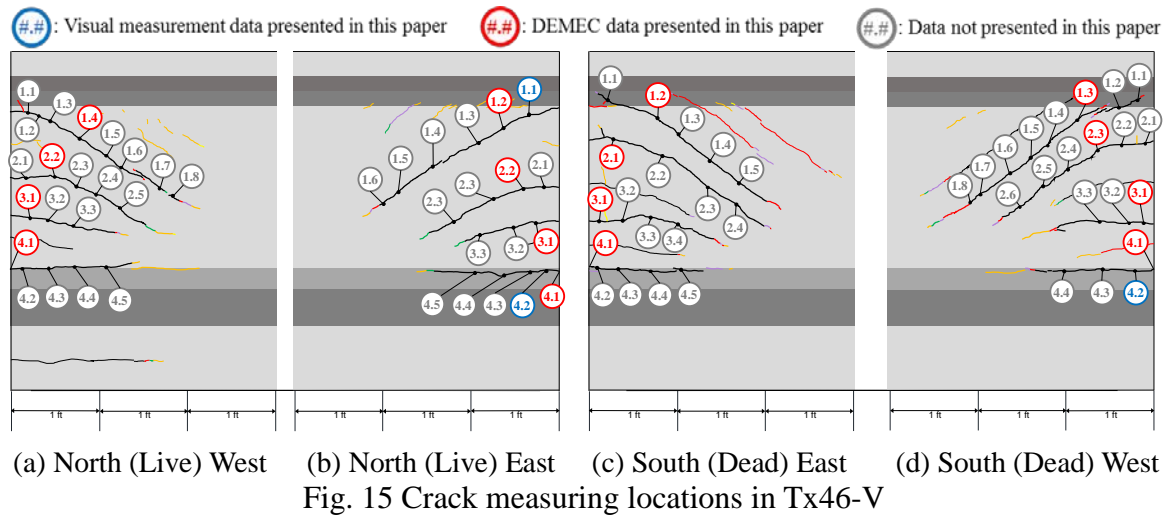
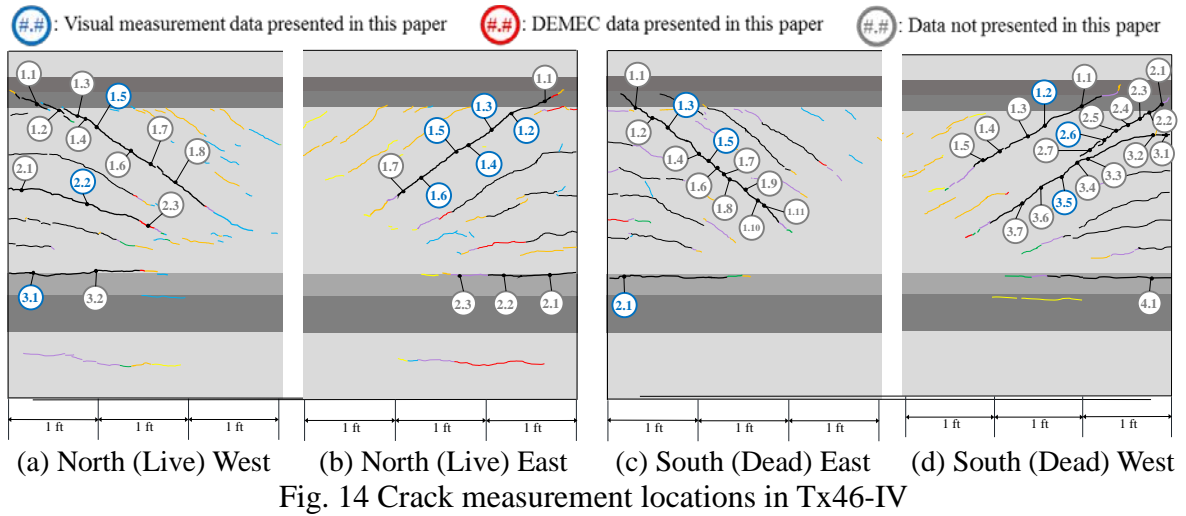


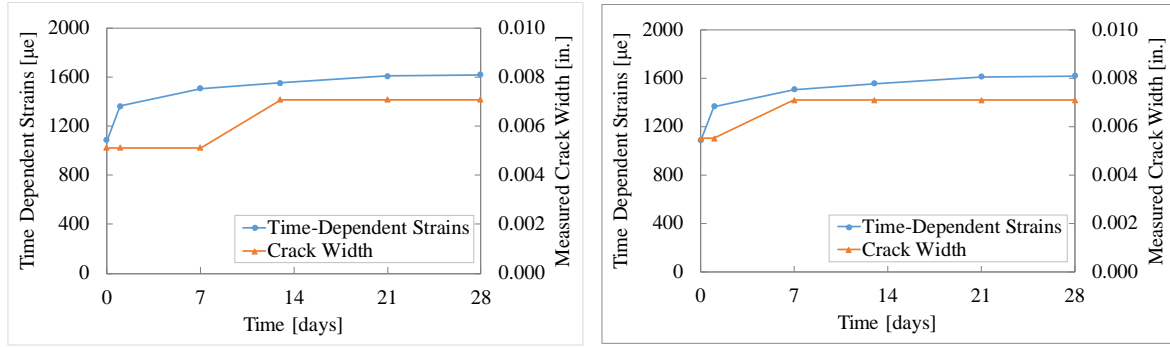
Fig 13. Crack measurement locations in Tx70-II



As previously noted, a series of VWGs was installed at the midspan of each specimen to measure the time-dependent changes in strains due to creep and shrinkage. The readings obtained from these gauges were used to establish a linear strain profile and estimate the strain changes throughout the depth of the specimens.

Fig. 16 through Fig. 18 present the observed growth in the widths of widest spalling cracks within the end-regions of each specimen in comparison with the measured time-dependent strain at the centroid of prestressing strands at the midspan of that specimen. The cracks in these figures are identified with the notation that was introduced in Fig. 13 through Fig. 15.

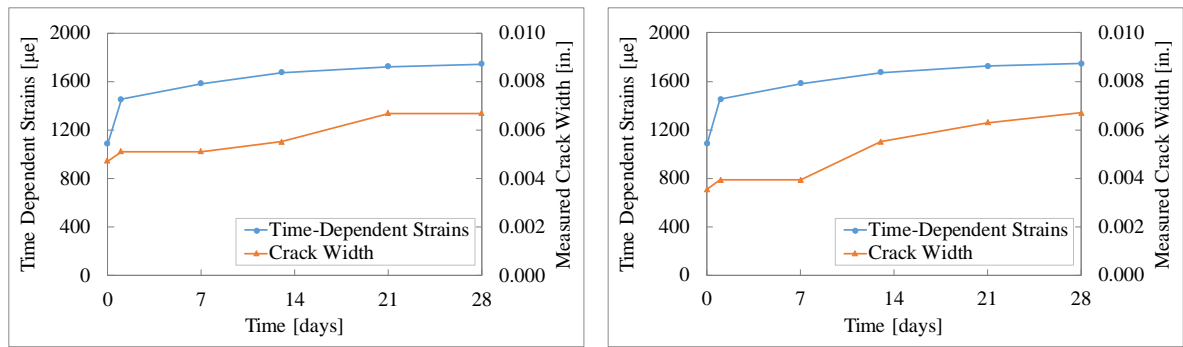
Fig. 16 through Fig. 18 show a clear correlation between the widths of inclined spalling cracks and time-dependent strains. Over the 28-day period of measurements, the growth in the width of the widest spalling crack was 34 percent for Tx70-II, 65 percent for Tx46-IV, and 53 percent for Tx46-V. During this period, the increases in strains at the centroid of strands at midspan were 49, 60, and 55 percent for Tx70-II, Tx46-IV, and Tx46-V, respectively.



(a) Live End (Crack: NE-1.1)

(b) Dead End (Crack: SE-1.3)

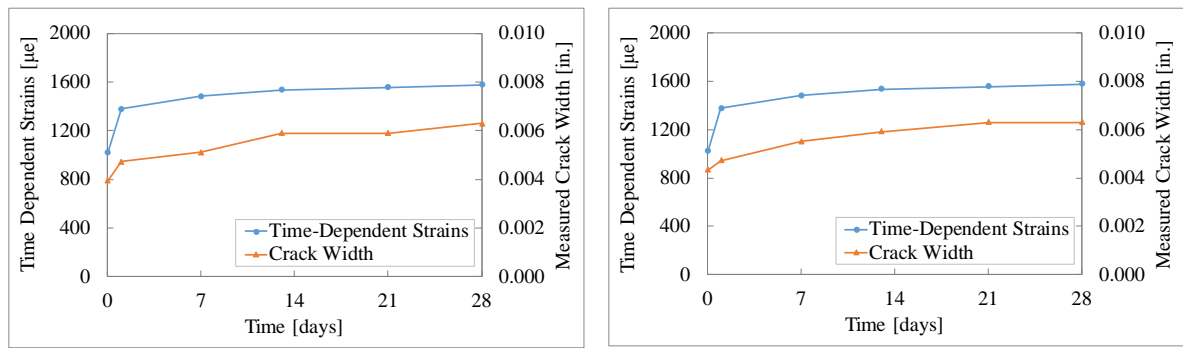
Fig. 16 Time-dependent changes in strains and widths of spalling cracks in Tx70-II



(a) Live End (Crack: NE-1.3)

(b) Dead End (Crack: SW-2.6)

Fig. 17 Time-dependent changes in strains and widths of spalling cracks in Tx46-IV

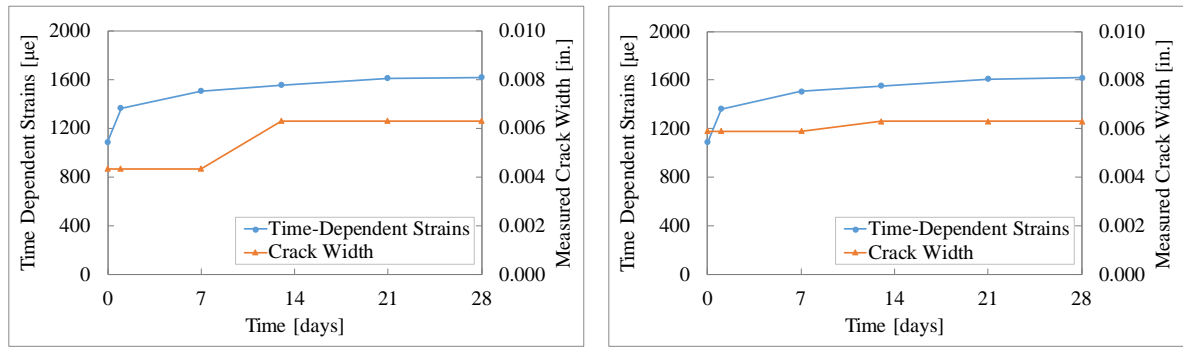


(a) Live End (Crack: NE-1.1)

(b) Dead End (Crack: SW-1.3)

Fig. 18 Time-dependent changes in strains and widths of spalling cracks in Tx46-V

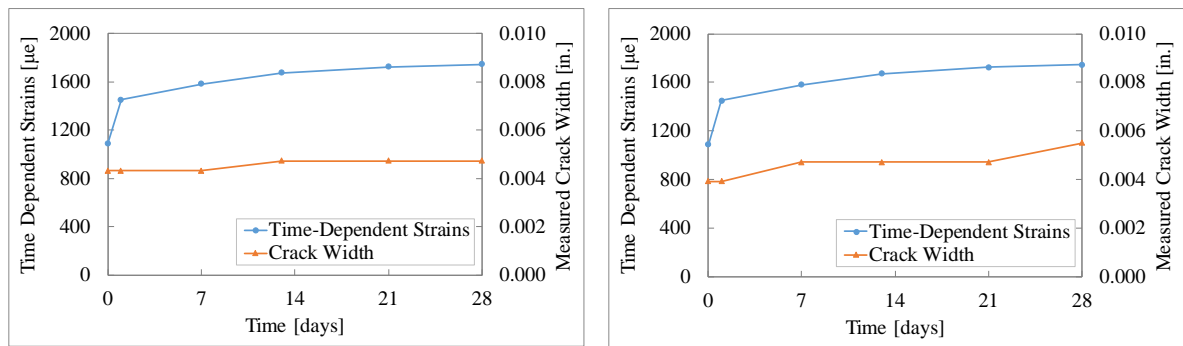
A similar comparison is made between the trends of time-dependent strains and the widths of interface cracks, i.e. cracks at the interface between the web and the bottom flange, in Fig. 19 through Fig. 21. As can be seen in these figures, a slight increase was observed in the widths of interface cracks over time. However, these cracks do not appear to be as sensitive as the spalling cracks to time-dependent strain changes, and the trends for time-dependent strains and crack widths are not well correlated. Over the 28-day period of measurements, the growth in the width of the interface cracks was 26 percent for Tx70-II, 25 percent for Tx46-IV, and 20 percent for Tx46-V.



(a) Live End (Crack: NE-2.1)

(b) Dead End (Crack: SW-2.1)

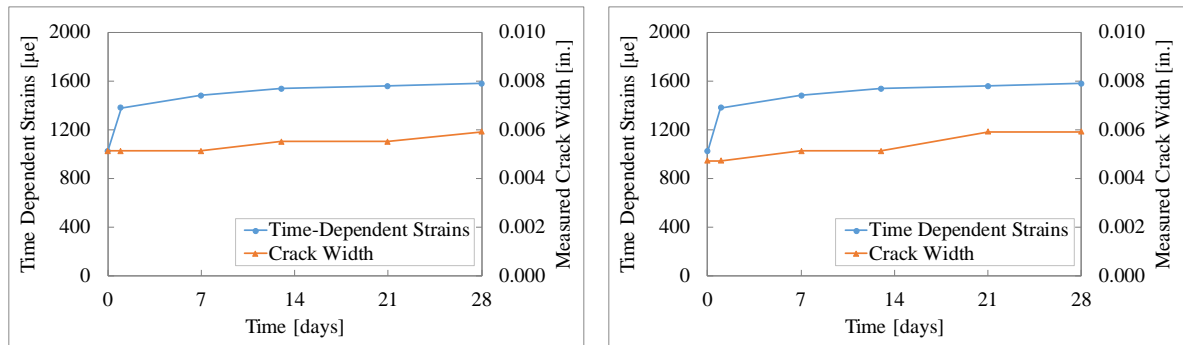
Fig. 19 Time-dependent changes in strains and the width of interface crack in Tx70-II



(a) Live End (Crack: NW-3.1)

(b) Dead End (Crack: SE-2.1)

Fig. 20 Time-dependent changes in strains and the width of interface crack in Tx46-IV



(a) Live End (Crack: NE-4.2)

(b) Dead End (Crack: SW-4.2)

Fig. 21 Time-dependent changes in strains and the width of interface crack in Tx46-V

CHANGES IN END-REGION CRACKS UNDER LOAD

Fig. 22 shows changes in the widths of end-region cracks during the shear testing of Tx46-IV. The figure shows a noticeable and consistent reduction in the crack widths within both end-regions of the specimen with the increase in the applied load. Most end-region cracks were observed to close almost completely when first diagonal cracking was observed, after which the rate of reduction in the crack widths decreased significantly for the remaining cracks.

Similar observations were made from Tx46-V. In this specimen, which was extensively monitored for crack widths during the shear testing, only small changes were detected in the widths of end-region cracks after first diagonal cracking had occurred at an applied load of 545 kips.

While all cracks showed a reduction in their widths due to applied load, the rate of decrease in the width of end-region cracks and the load at which noticeable changes were first observed in crack widths were dependent on the location of the crack. In general, cracks near the top of the web started to close at a greater applied load compared to those at the bottom of the web. For example, in Tx46-IV, the width of SE-1.3 started to reduce at a greater applied load than that of SW-3.5, as shown in Fig. 22b. This observation is expected, as compressive stresses gradually expand into the web from the support, and as a result, the magnitude of compressive stresses that can help close the spalling cracks in the upper portions of the web over the supports is small. A distributed loading condition is more likely to represent the loading conditions of a bridge girder. In distributed loading condition, it is expected that a greater compressive force be transferred through the web in the regions directly over the supports. As a result, cracks within the upper portions of the web are expected to close more quickly than observed in the current testing program under point loading.

The DEMEC measurements obtained from Tx46-V showed similar trends, as shown in Fig. 23. The crack widths in this figure are calculated based on the simplifying assumption that all of the measured strain is related to the reduction in the width of cracks. Fig. 23 shows that the crack widths tend to stabilize after a load level of approximately 700 kips. Visual observations from all cracks in this specimen showed that the width of end-region cracks was limited to 0.005 in. at this load level.

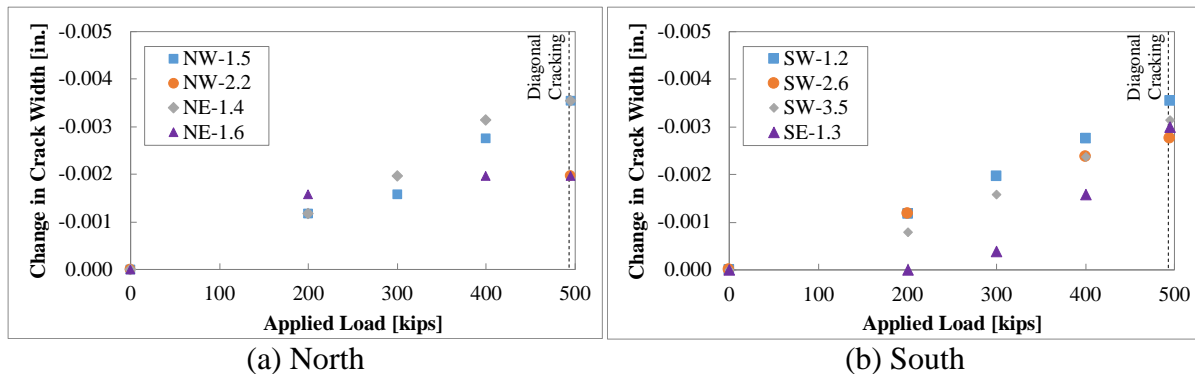


Fig. 22 Changes in the widths of end-region cracks in Tx46-IV during shear test, based on visual measurement

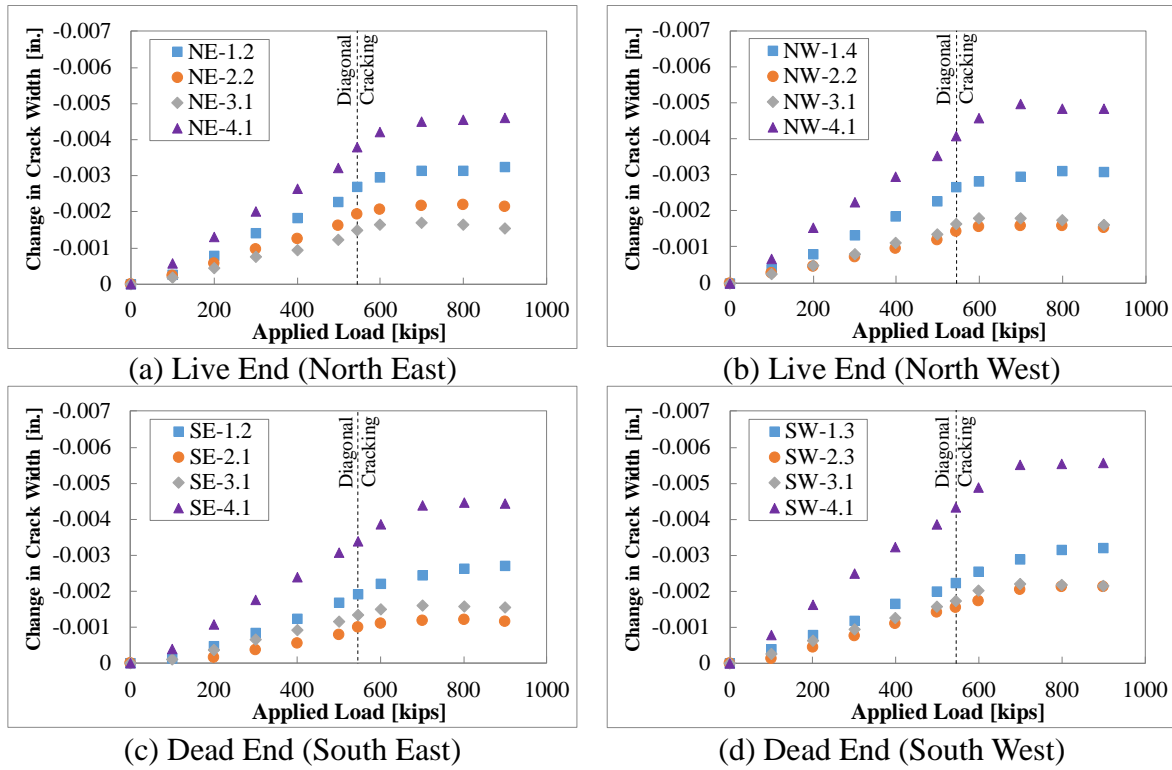


Fig. 23 Changes in the widths of end-region cracks in Tx46-V during shear test, based on DEMEC measurements

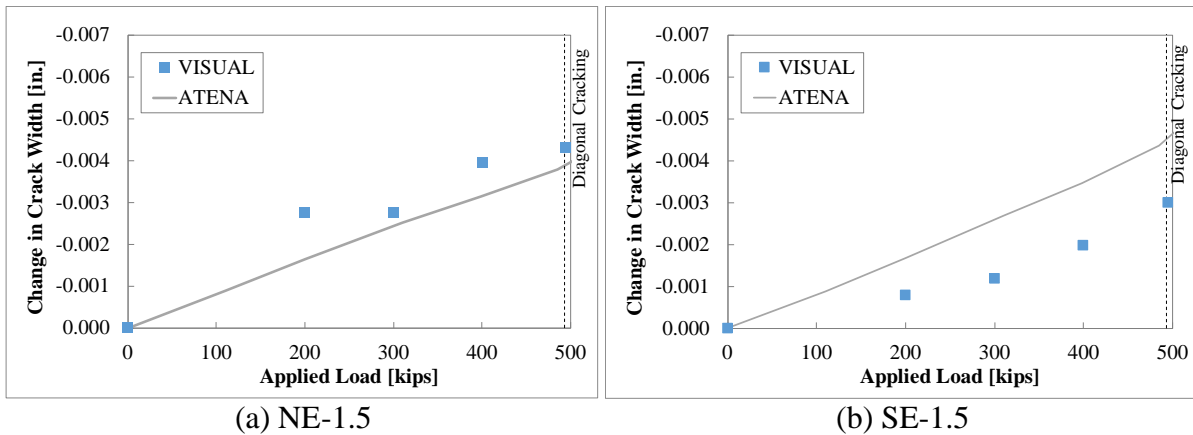


Fig. 24 Comparison between FE results and visual measurements of crack widths for Tx46-IV

Fig. 24 and Fig. 25 provide a comparison between the results of FEA and select measurements of crack widths from Tx46-IV and Tx46-V, respectively. As can be seen in the figures, FE models of the girders were generally successful in capturing the trends of changes in crack widths under load. Before the first diagonal shear cracking, the absolute values of changes in crack widths obtained from ATENA were also in good agreement with those obtained from DEMEC measurements for Tx46-V. It is visible in the figure that the absolute crack widths in the girder differed from the estimates obtained from ATENA. This comes as no surprise,

because the actual crack widths may change depending on a variety of parameters, including the temperature, curing conditions of the girder, properties of aggregates, and location of the measurements. The material models used in ATENA to estimate tensile and fracture properties of concrete are also based on a variety of simplifying assumptions that will certainly contribute to some level of error in crack width estimations. Therefore, it is not expected that reliable absolute crack widths be obtained from FEA models. However, the results from such models can be used to investigate the cracking patterns and how the crack widths may change under applied loads.

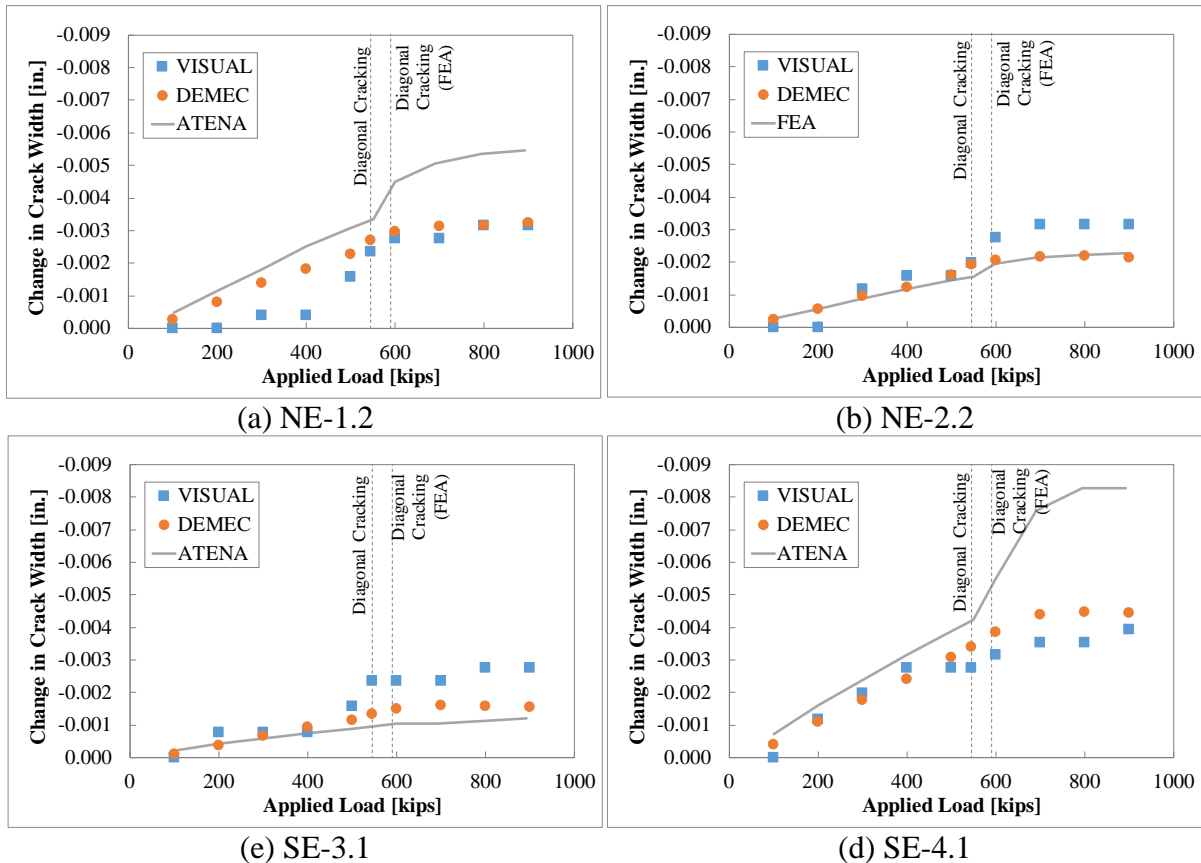


Fig. 25 Comparison between FE results and measurements of crack widths for Tx46-V

The observed reduction in crack widths was consistent with the strain changes in the stirrups within the end-region, as shown in Fig. 26 and Fig. 27. In these figures, the data recorded from the closest strain gauge to the location of the monitored crack are presented together with the observed crack widths.

Before the appearance of the first diagonal shear crack, most stirrups in the end-region were subjected to an almost linear increase in compressive stresses due to applied loads, which corresponds to a reduction in the width of end-region cracks. After the first diagonal cracking, however, stresses in the stirrups and the width of end-region cracks tend to stabilize and reach a plateau.

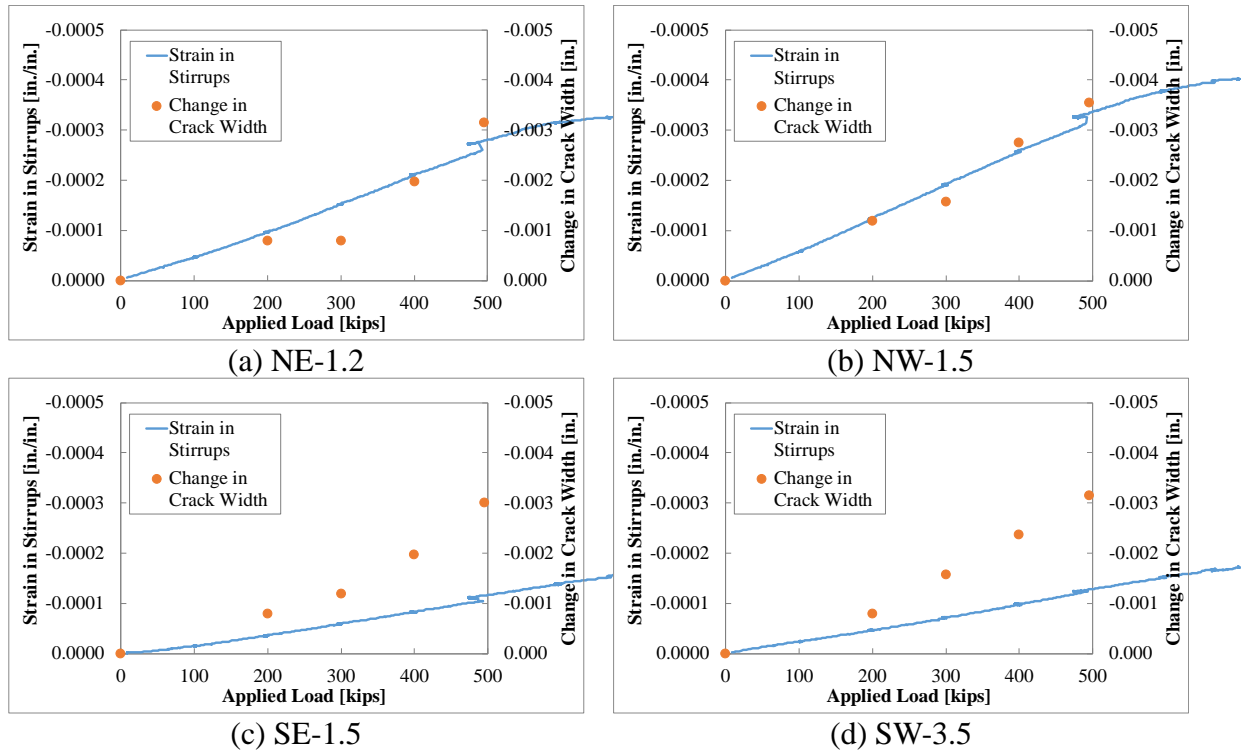


Fig. 26 Comparison between changes in crack width by visual measurement and stress in stirrups in the end-region of Tx46-IV during shear test

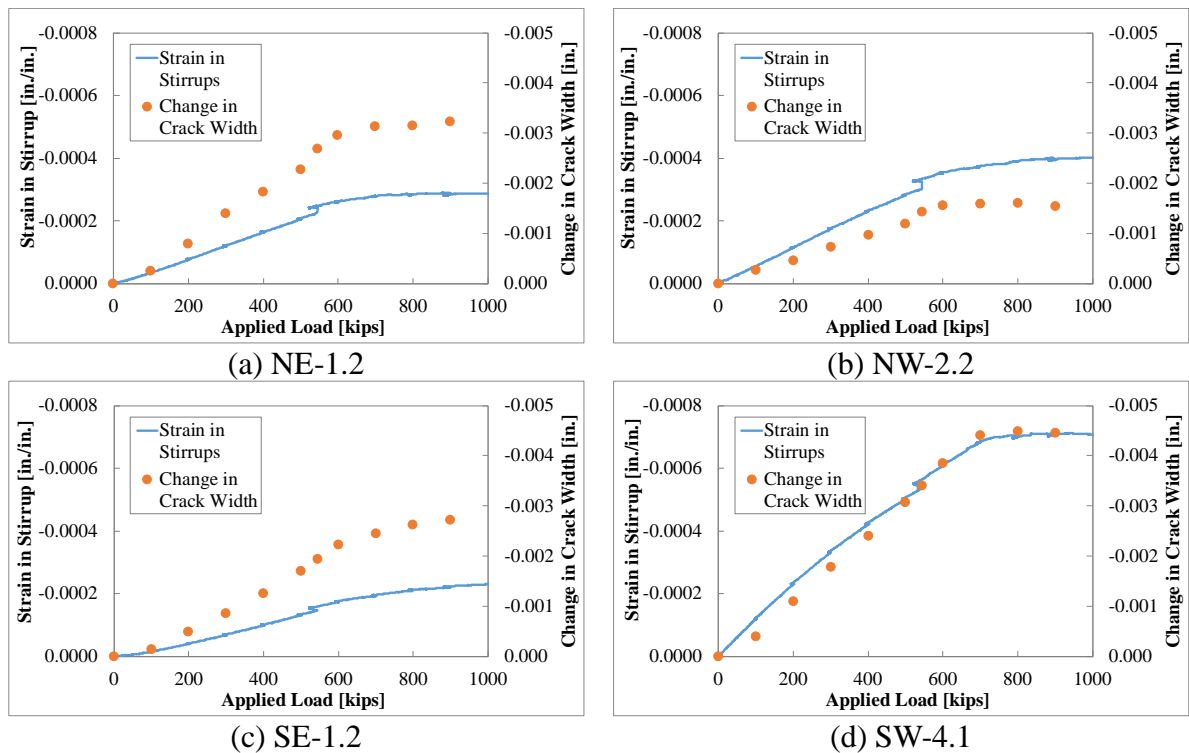


Fig. 27 Comparison between changes in crack width based on DEMEC measurements and stress in stirrups in the end-region of Tx46-IV during shear test

CONCLUSION

This paper focused on examining changes in the end-region cracks of pretensioned girders fabricated with 0.7-in. diameter strands, due to time-dependent effects and applied loads. The results presented herein included the measurements obtained from a series of full-scale specimens, as well as results from finite-element simulations of pretensioned girders in ATENA.

Measurements from three full-scale specimens over the 28-day monitoring period showed that end-regions cracks due to prestress transfer continue to grow in length, width, and number over time. This is primarily due to time-dependent deformations of the concrete such as creep and shrinkage. An increase up to 65 percent was observed in the widths of some cracks over the first 28 days, which is a significant change that must be taken into account when defining acceptable crack widths at release. Typically, spalling cracks in the web had a tendency to grow more over time compared to those at the interface between the web and bottom flange.

Observations from shear-critical loading tests showed that end-region cracks start to close under relatively small applied loads. The results obtained from DEMEC measurements, which were in agreement with observations from FEA results, showed that these cracks decreased by up to 0.006 in. in width. The cracks did not close completely before the first diagonal shear crack developed. However, it is evident that the two faces on either side of the crack close enough to bear against each other across the width of the web. Therefore, pretensioned girders that develop end-region cracks at prestress transfer may have narrower cracks once the girder has been placed in service-load conditions. In other words, some pretensioned concrete girders that may require repair based on observed conditions immediately after release could eventually have tolerable crack widths when placed in the actual bridge configuration.

The work presented in this paper is a part of an ongoing effort. Future work on this topic includes investigation of results from a variety of other specimens as well as outputs of parametric finite-element simulations to evaluate the acceptance criteria for the widths of end-region cracks in pretensioned girders to prevent durability issues while eliminating unnecessary repairs.

ACKNOWLEDGEMENTS

The authors gratefully acknowledge the Texas Department of Transportation (TxDOT) for providing financial support for this study. Moreover, the authors would like to thank Coreslab Structures for donating the concrete used for all of specimens presented in this paper. The findings, opinions, and recommendations presented in this article are those of the authors and do not necessarily reflect the views of TxDOT.

REFERENCES

1. Tadros, M. K., Badie, S. S., and Tuan, C. Y., "Evaluation and Repair Procedures for Precast/Prestressed Concrete Girders with Longitudinal Cracking in the Web," NCHRP Report 654, Transportation Research Board, Washington D.C, 2010.
2. Nawy, E. G., "Crack Control in Reinforced Concrete Structures," ACI JOURNAL, Proceedings V. 65, No. 10, Oct. 1968, pp. 825-836.
3. Halvorsen G.T., "Code requirements for crack control," Concrete and Concrete Construction, ACI SP-104, American Concrete Institute, Farmington Hills, Michigan, 1987. pp. 275-322.
4. Precast/Prestressed Concrete Institute (PCI), Manual for the Evaluation and Repair of Precast, Prestressed Concrete Bridge Products, Publication MNL-37-06, Precast/Prestressed Concrete Institute, Chicago, IL, 2006.
5. Schiessl, P., "Admissible Crack Width in Reinforced Concrete Structures," Preliminary Report, Vol. 2 of IABSE-FIP-CEB-RILEM-IASS, Colloquium, Liege, 1975.
6. Salazar, J., Yousefpour, H., Alirezaei Abyaneh, R., Kim, H., Katz, A., Hrynyk, T., and Bayrak O., "End-Region Behavior of Pretensioned I-Girders Employing 0.7-in. (17.8-mm) Strands", ACI Structural Journal (Accepted, in press), 2017.
7. Katz, A., Yousefpour, H., Kim, H., Alirezaei Abyaneh, R., Salazar, J., Hrynyk, T., and Bayrak, O., "Shear Performance of Pretensioned Concrete I-Girders Employing 0.7-in. (17.8-mm) Strands", ACI Structural Journal, V. 114, No. 5, September/October 2017, pp 1273-1284.
8. Kim, H., Katz, A., Salazar, J., Abyaneh, R., Yousefpour, H., Hrynyk, T., and Bayrak, O., "End-Region Serviceability and Shear Strength of Precast, Pretensioned I-Girders Employing 0.7-in. Diameter Strands," PCI/NBC, Cleveland, OH, 2017.
9. Hanson, N. W., "Influence of Surface Roughness of Prestressing Strand in Bond Performance," PCI Journal, V. 14, No. 1, January/February 1969, pp. 32-45.
10. Kaar, P. H., LaFraugh, R. W., and Mass, M. A., "Influence of Concrete Strength on Strand Transfer Length," PCI Journal, V. 8, No. 5, 1963, pp. 47-67.
11. Barnes, R.W., Burns, N.H., and Kreger, M. E., "Development of Length of 0.6- Inch Prestressing Strand in Standard I-shaped Pretensioned Concrete Beams," in Research Report. 1999: Austin, TX.
12. Salazar, J., Yousefpour, H., Katz, A., Abyaneh, R., Kim, H., Garber, D., Hrynyk, T., and Bayrak, O., "Benefits of Using 0.7 inch (18 mm) Strands in Precast, Pretensioned Girders: a Parametric Investigation," PCI Journal, November/December 2017, pp 61-77.
13. American Association of State Highway and Transportation Officials (AASHTO), "AASHTO LRFD Bridge Design Specifications", 7th Edition, with 2015 and 2016 Interim Revisions, Washington, D.C., 2016.
14. Texas Department of Transportation (TxDOT), "Concrete I-Girder Details," Standard Drawing by the Bridge Division, Austin, TX, 2015.
15. Červenka, J., and Procházková, Z., "ATENA Program Documentation- Part 4-2: Tutorial Texas Department of Transportation (TxDOT), "Concrete I-Girder Details," Standard for Program ATENA 3D," Červenka Consulting s.r.o., Prague, Czech Republic., 2013.
16. O'Callaghan M. R., "Tensile Stresses in the End Regions of Pretensioned I-Beams at Release," Master's Thesis, University of Texas at Austin, Austin, TX, 2007.

17. Tadros, M. K. and Morcous, G., "Impact of 0.7 inch Diameter Strands on NU I-Girders," Technical Report: Nebraska Department of Roads, Lincoln, NE, 2011.
18. ASTM, "ASTM A370: Standard Test Methods and Definitions for Mechanical Testing of Steel Products," ASTM, West Conshohocken, PA, 2016.
19. Bigaj, A. J., "Structural Dependence of Rotations Capacity of Plastic Hinges in RC Beams and Slabs," Delft University of Technology, Delft, the Netherlands, 1999.
20. ACI Committee 224, "Control of Cracking in Concrete Structures (ACI 224R-01)," American Concrete Institute, Farmington Hills, MI, 2001.